



Pergamon

Available online at [www.sciencedirect.com](http://www.sciencedirect.com)

SCIENCE @ DIRECT®

OCEAN  
ENGINEERING

Ocean Engineering 30 (2003) 1117–1135

[www.elsevier.com/locate/oceaneng](http://www.elsevier.com/locate/oceaneng)

# Three-dimensional hydrodynamic model, study cases for quarter annular and idealized ship channel problems

W.W. Pandoe \*, B.L. Edge

*Ocean Engineering Program, Department of Civil Engineering, Texas A&M University, College Station Texas 77843-3136, USA*

Received 21 June 2002; accepted 2 July 2002

---

## Abstract

An extended version of the three-dimensional hydrodynamic model, ADCIRC 3D-DSS, was utilized to simulate both horizontal and vertical flows in a (quarter) annular harbor (QATP and ATP) and rectangular basin with an idealized ship channel (RBSC). Comparison of horizontal and vertical solutions to the analytical solution and results of other researchers are in good agreement. The vertical velocity solution is highly sensitive to the horizontal velocity solutions. The presence of the sidewall boundary may also affect the vertical solutions. Around the sloping bank of RBSC channel with one-third gradient, the vertical velocity becomes important. The maximum vertical velocity approaches  $\pm 50\%$  of the sediment fall velocity of fine sand.

© 2002 Elsevier Science Ltd. All rights reserved.

*Keywords* Three-dimensional; Finite element method; Vertical velocity; Ship channel

---

## 1. Introduction

Over the past several years, a large number of hydrodynamic numerical models have been reported (Luettich et al., 1992a; Martin and McCutcheon, 1998; Mellor, 1998). The basic theme is to provide robust and comprehensive hydrodynamic circu-

---

\* Corresponding author. Tel.: +1-979-845-0273; fax: +1-979-862-8162.  
E-mail address: [wpandoe@tamu.edu](mailto:wpandoe@tamu.edu) (W.W. Pandoe).

lation and transport models for use in pursuit of specific, focused engineering and scientific investigations. Development of coastal engineering projects, such as coastal management, dredging work, coastal protection, ship channel maintenance and sustainable coastal development requires a detailed knowledge of the hydrodynamic circulation. Some numerical models based on the two- or three-dimensional models have been widely developed.

The scope of this paper is to implement and expand the hydrodynamic numerical modeling system for the idealized ship channel as a step toward a natural harbor configuration. The model used is the Advanced Circulation Model (ADCIRC) originally developed in the early 1990's (Luettich et al., 1992a,b). ADCIRC is a two and three dimensional finite element model used for hydrodynamic circulation problems. The model is based on the finite element codes that solve the shallow water equation on unstructured grids. The finite element formulation has the advantage of flexibility in resolution over the area domain. Fine resolution can be specified locally to meet the accuracy requirements, and coarse resolution can be implemented in areas distant from the region of interest.

Grenier et al. (1995) studied a comparison between the two-dimensional depth-integrated (2DDI) and three-dimensional (3D-DSS) of ADCIRC models. The ADCIRC 2DDI is a two-dimensional depth-integrated model that solves sea surface elevation  $\eta$  and depth-averaged velocity  $U$  and  $V$ . The model has been successfully implemented for estuaries, tidal inlets, navigation channel, harbor embayments and many other coastal problems. The three-dimensional model, ADCIRC 3D-DSS, applies a mode-splitting technique to solve the vertical profile of horizontal velocity by discretizing the shear stress (Luettich et al., 1992a; Luettich et al., 1994). This model is called a direct stress solution or DSS. The original version of 3D-DSS model does not provide a vertical velocity solution; it only provides a vertical distribution of the horizontal flows. Thus, an additional subroutine, called WSSOL, is newly developed by the authors in conjunction with the existing 3D-DSS model, which completes the model for solving three-dimensional flow fields  $u$ ,  $v$  and  $w$ .

Muccino et al. (1997) reported the development of methods for solving vertical velocity. Their results are consistent with the analytical solutions. However, the elevation and horizontal velocity applied to compute the vertical velocity are obtained from the three-dimensional diagnostic model FUNDY5. In this paper the adjoint method is implemented in ADCIRC 3D-DSS model for solving the vertical velocity.

Solving horizontal and vertical velocities three-dimensionally is necessary for explaining the variability of the current shear, which may alter the velocity distribution vertically. Three-dimensional solution of the hydrodynamic flow can explain the relationship between periodic tide and the currents within the area of study. This may lead to an explanation of both divergence and convergence zones and corresponding depositional area.

As in Muccino et al. (1997) the quarter annular test problem (QATP) is used for a test case and the results are in good agreement with the analytical solution. An interesting observation is the vertical velocity that affects the general flow pattern in an idealized ship channel. The effect of a sloping bank on both sides of the channel generates an up- and down-flow pattern associated with the induced tidal period.

## 2. Mathematical model

This study was performed using the ADCIRC 3D-DSS circulation model that includes both two-dimensional depth integrated and three-dimensional solutions. The mathematical model of hydrodynamic circulation in coastal water is based on the three-dimensional Navier–Stokes equations. The detailed explanations of the model are given in Luettich et al. (1992a); Luettich et al. (1994), and Luettich and Westerink (2001). A summary of governing equations of three-dimensional circulation is given in the following paragraphs.

### 2.1 Governing equations

The computation of hydrodynamics is performed in a sigma ( $\sigma$ )-coordinate system. The main governing equations follow:

- continuity equation

$$\frac{\partial \eta}{\partial t} + \frac{\partial uH}{\partial x} + \frac{\partial vH}{\partial y} + (a-b)\frac{\partial \omega}{\partial \sigma} = 0 \quad (1)$$

- Momentum equations in the longitudinal and lateral directions:

$$\begin{aligned} \frac{\partial u}{\partial t} + u\frac{\partial u}{\partial x} + v\frac{\partial u}{\partial y} + \omega\left(\frac{a-b}{H}\right)\frac{\partial u}{\partial \sigma} - fv = -\frac{\partial}{\partial x}\left[\frac{p_s}{\rho_0} + g(\zeta - \alpha\eta)\right] + m_{x\sigma} \\ - b_{x\sigma} + \left(\frac{a-b}{H}\right)\frac{\partial}{\partial \sigma}\left(\frac{\tau_{zx}}{\rho_0}\right) \end{aligned} \quad (2a)$$

$$\begin{aligned} \frac{\partial v}{\partial t} + u\frac{\partial v}{\partial x} + v\frac{\partial v}{\partial y} + \omega\left(\frac{a-b}{H}\right)\frac{\partial v}{\partial \sigma} + fu = -\frac{\partial}{\partial x}\left[\frac{p_s}{\rho_0} + g(\zeta - \alpha\eta)\right] + m_{y\sigma} \\ - b_{y\sigma} + \left(\frac{a-b}{H}\right)\frac{\partial}{\partial \sigma}\left(\frac{\tau_{zy}}{\rho_0}\right) \end{aligned} \quad (2b)$$

where  $u$  and  $v$  are depth-dependent horizontal velocity,  $\omega$  is vertical velocity in sigma ( $\sigma$ ) coordinate system,  $\eta$  is a free surface elevation,  $p_{s(x,y,z)}$  is a time-averaged pressure,  $f$  is the Coriolis force,  $m_i$  is a horizontal momentum diffusion,  $b_i$  is a baroclinic pressure gradient,  $\tau_{zi}$  is a combined viscous and turbulent Reynolds stress and  $\rho_0$  represents reference sea water density.

The equations above are defined in  $\sigma$ -coordinate system, where  $\sigma$  is defined by:

$$\sigma \equiv a + \frac{(a-b)(\eta-z)}{H} \quad (3)$$

where  $H = \eta + h$  = total water depth to the free surface, and in ADCIRC the value of  $a = 1$  and  $b = -1$ .

## 2.2. Solving horizontal velocity $u(\sigma)$ and $v(\sigma)$

The computation of horizontal velocities is also performed in the  $\sigma$  coordinate system following the 3D-DSS governing equations. The solution strategy was developed by discretizing the shear stress equation, later called direct stress solution (DSS). The complete formulations of the 3D-DSS model are explained in detail by Luetlich et al. (1994), where the horizontal advective and diffusion terms are neglected. Velocity is obtained by taking the vertical derivative of the momentum equations. The inverted standard eddy viscosity ( $E_z$ ) can be expressed as:

$$\frac{\partial u}{\partial \sigma} = \frac{H}{(a-b)E_z \rho_o} \tau_{zx} \quad (4a)$$

$$\frac{\partial v}{\partial \sigma} = \frac{H}{(a-b)E_z \rho_o} \tau_{zy} \quad (4b)$$

Since ADCIRC uses a terrain following  $\sigma$ -coordinate system, solution for horizontal velocity by integrating eq (4) from the bottom ( $\sigma = b$ ) to the surface ( $\sigma = a$ ) is:

$$u(\sigma) = u_b + \frac{H}{(a-b)} \int_b^\sigma \frac{\tau_{zx}}{E_z \rho_o} d\sigma \quad (5a)$$

$$v(\sigma) = v_b + \frac{H}{(a-b)} \int_b^\sigma \frac{\tau_{zy}}{E_z \rho_o} d\sigma \quad (5b)$$

where  $u_b$  and  $v_b$  are the components of bottom slip velocities, which are determined by:

$$u_b = \frac{\tau_{bx}}{\rho_o k} \text{ and } v_b = \frac{\tau_{by}}{\rho_o k} \quad (6)$$

where  $\tau_{bx}$  and  $\tau_{by}$  are the bottom stress components;  $\tau_{zx}$  and  $\tau_{zy}$  are the components of vertical shear stress, and  $k$  is a slip coefficient. For the case of no-slip ( $k \rightarrow \infty$ ),  $u_b$  and  $v_b$  become zero.

## 2.3. Solving vertical velocity $w(z)$

The vertical velocity is solved by the first derivative approach with the adjoint correction. The equation is solved for  $\omega$  in sigma  $\sigma$ -coordinate. Let:

$$Q_\sigma = \frac{\partial \eta}{\partial t} + \frac{\partial(u_\sigma H)}{\partial x} + \frac{\partial(v_\sigma H)}{\partial y} \quad (7)$$

with essential boundary condition  $\omega = 0$  at  $\sigma = b$ , and natural boundary condition  $\delta\omega = 0$  at  $\sigma = a$ . Integrating both sides with respect to  $\sigma$  from  $a$  to  $b$  yields:

$$\omega_{m+1} - \omega_m = -\frac{1}{(a-b)} \int_m^{m+1} Q_\sigma \partial \sigma \tag{8}$$

where  $m$  is a node number over vertical element. The solution  $\omega_m$  will satisfy the bottom boundary condition only. In order to satisfy the free surface, the adjoint correction is applied based on Luetlich and Muccino (2001):

$$\omega_{adj} = \omega_\sigma - \omega_\sigma(\eta) \left[ \frac{(\sigma-b) + \frac{HL}{a-b}}{(a-b) + \frac{2HL}{a-b}} \right] \tag{9}$$

where  $\omega_\sigma(\eta)$  is the misfit of surface boundary condition at the free surface  $\eta$ , and  $L$  is the weight of the relative contribution of the boundary conditions versus the interior solution. The value  $L = 0$  is applied to the resulting  $\omega_\sigma$  which is equal to adding a linear correction to the 1st order derivative equation that satisfies only the bottom boundary condition ( $\omega_\sigma = 0$  at  $\sigma = b$ ). This adjoint correction will give the solution exactly at the surface boundary condition, which in this case  $\omega_{adj} = 0$  at  $\sigma = a$ .

The corresponding conversion of vertical velocity from sigma-level ( $\omega$ ) to  $z$ -level ( $w$ ) is also given by Luetlich and Muccino (2001):

$$w = \omega + \left(\frac{\sigma-b}{a-b}\right) \frac{\partial \eta}{\partial t} + u \left[ \left(\frac{\sigma-b}{a-b}\right) \frac{\partial \eta}{\partial x} + \left(\frac{\sigma-a}{a-b}\right) \frac{\partial h}{\partial x} \right] + v \left[ \left(\frac{\sigma-b}{a-b}\right) \frac{\partial \eta}{\partial y} + \left(\frac{\sigma-a}{a-b}\right) \frac{\partial h}{\partial y} \right] \tag{10}$$

The approach of computation follows three main steps: (1) compute the  $\omega$  in  $\sigma$ -coordinate system with the output written to the fort 102 unit file; (2) apply adjoint correction in  $\sigma$ -level; and (3) transform  $\omega$  from  $\sigma$ -coordinate into  $w$  in  $z$ -coordinate system. The final output is written to fort 122 unit file for vertical velocity solution only, and also written to fort 124 unit file for global 3D velocity solutions  $u$ ,  $v$  and  $w$ . One may obtain both vertical velocity solutions in either  $\sigma$ -coordinate or  $z$ -coordinate systems.

ADCIRC 3D, version 36.01, also performs the computation of vertical velocity based on the ADCIRC 3D-VS model. The 3D-VS model is another version of the ADCIRC 3D that requires discrete representation of the horizontal velocity and so-called velocity solution or VS (Grenier et al., 1995). In the 3D-VS approach, computation of vertical velocity is carried out on the  $z$ -level directly by combining eqs (7)–(10) simultaneously. More detailed presentations of the model are given by Luetlich and Westerink (2001). The output of vertical velocity solution in  $\sigma$ -coordinate system is not available in this version.

Both 3D-DSS and 3D-VS use different approaches for solving the three-dimen-

sional flow fields. Comparison between them needs to be further investigated. The need of having vertical velocity solution in  $\sigma$ -coordinate is very important in the newly extended 3D-DSS model that will be used for future development of a transport model. The authors will use the 3D-DSS for the next step in development of a transport model that will also be performed in  $\sigma$ -coordinate system.

### 3. Study cases

Three example cases will be presented in this paper: (1) the quarter annular harbor test problem (QATP), (2) the annular test problem (ATP), and (3) the idealized ship channel in a rectangular sloped basin (RBSC). The QATP and ATP cases include analytical solutions where the formulations are provided in the appendices of Muccino et al. (1997) and Luettich et al. (2002). All cases were driven by one tidal component, the M2 periodic boundary forcing, with the amplitude of 0.1 m for QATP and ATP cases, and 0.5 m for the RBSC.

#### 3.1 The quarter annular harbor problem

The quarter annular harbor (QATP) has a quadratic bathymetry as shown in Fig. 1. The results obtained from ADCIRC model are compared to the analytical solution, as investigated by Muccino et al. (1997) and Luettich et al. (2002). The geometry of the grid is shown in Fig. 1.

The QATP grid, generated by SMS Water Modeling System version 7.0, as shown in Fig. 1, consists of 825 nodal points and 1536 triangular elements. The open boundary, located at  $r_2 = 100$  km, is defined along the outer perimeter with uniform depth of 62.5 m, and with 33 open boundary nodes. This boundary is forced by an M2 tide with frequency  $\omega = 1.40518917083 \times 10^{-4} \text{ s}^{-1}$  and amplitude of 0.1 m. One land boundary is also defined along the inner perimeter at  $r_1 = 40$  km and both lateral boundaries  $\theta = 0$  and  $\theta = \pi/2$ . This land boundary consists of 81 land boundary nodes. ADCIRC allows an optional internal boundary with no normal flow as an essential boundary condition and allowing free tangential slip (IBTYPE=1).

For the vertical configuration of the QATP case, a no-slip bottom boundary condition is applied, and consequently the slip coefficient  $k \rightarrow \infty$ . To satisfy eq. (6),  $u_b$  and  $v_b$  become zero. The selected free surface roughness is 0.0001, and the bottom roughness is 0.015 (constant horizontally). Finite element vertical grid contains 9 nodes vertically at  $\sigma$ -values from bottom-up:  $-1.0, -0.87, -0.71, -0.5, 0.0, 0.5, 0.71, 0.87$  and  $1.0$ . The selected model of eddy viscosity varies linearly over the lower 20% of the water depth and remains constant in the upper 80% of the water depth.

#### 3.2 The annular harbor problem

The annular test problem was also presented accompanying the QATP case. Comparing to the QATP, the ATP is developed for further study of the effect of lateral

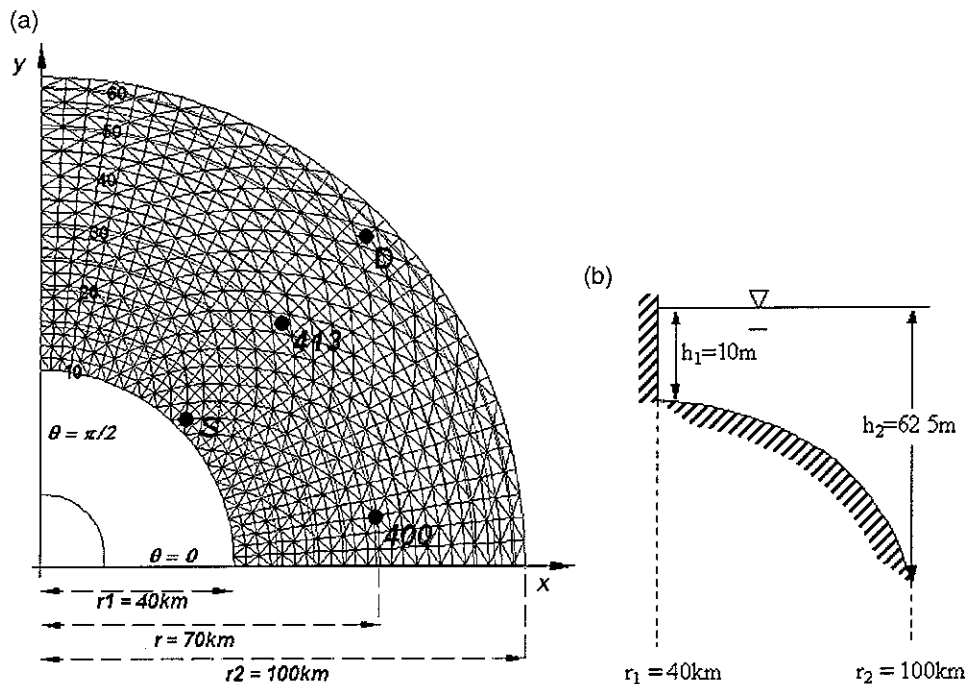


Fig. 1 (a) Top view of elements grid of quarter annular harbor test problem (QATP) Open boundary is defined at  $r = r_2$ , and closed boundaries are at  $\theta = 0$ ,  $\theta = \pi/2$  and  $r = r_1$  Black nodes indicate four selected points of interest (b) Side view of quarter annular harbor with minimum and maximum depths 10 m and 62.5 m, respectively The bottom profile follows quadratic bottom

boundaries as it was applied in QATP case. ATP eliminates the presence of lateral boundaries

The ATP grid, shown in Fig 2, contains 3200 nodal points and 6144 triangular elements The bathymetric profile and radial range are similar to the QATP, but with  $\theta = 0-2\pi$  circular angle instead of  $\theta = 0-\pi/2$  as in the QATP An open boundary is defined along the outer perimeter with uniform depth of 62.5 m, and with 128 open boundary nodes One land boundary is also defined along the inner perimeter and both lateral boundaries that consist of 128 land boundary nodes

### 3.3. The rectangular basin

The idealized sloped-rectangular basin with “ship” channel along the center near end of the basin is generated through SMS Water Modeling System version 7.0. The grid and contour plots of the basin are shown in Fig 3a and b, where the cross-channel has a slope at about 1:3 (Fig. 3c, section A) The channel has a length of 9 km, width of 625 m and a constant depth 10 m (Fig 3c, Section B) The minimum depth outside the channel is 5 m located near west end of the basin The coordinate system used for the grid is Cartesian

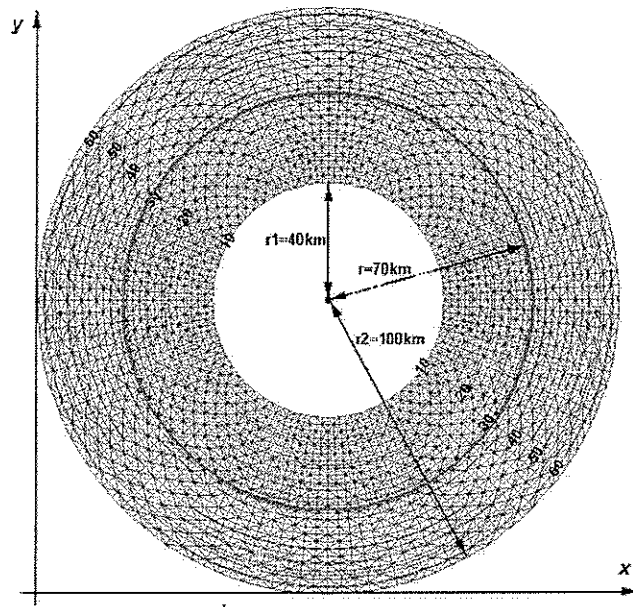


Fig. 2 Top view of annular harbor test problem (AIP) Bold circular line represents the selected radius of interest at  $r = 70 \text{ km}$ . The bottom profile is similar to the QATP (Fig. 1b)

An open boundary is defined along a section located in the west (left) end of the basin with uniform depth 20 m, and with 16 open boundary nodes. One land boundary is also defined along the east (right) end and two lateral sidewall boundaries are located on the north and south. The grid consists of 18 195 nodes and 36 231 triangular finite elements. Thirty-one recording stations are defined within the grid across the channel indicated as section A in Fig. 3. The model is run for 60 h (2.5 days), and is forced by one M2 tidal component with amplitude 0.5 m.

The vertical configuration of the grid are similar to the one used in both QATP and AIP, with 9 vertical nodes.

#### 4. Results and discussions

##### 4.1 QAIP and ATP test cases

The results of the three dimensional velocity components obtained from QATP and AIP are compared to the analytical solution. The three-dimensional analytical solution is available in Muccino et al. (1997), which was developed by Lynch and Officer (1985). Four points are selected in the QATP grid: node D ( $r = 95 \text{ km}$ ), 400 ( $r = 70 \text{ km}$ ,  $\theta = 8.4^\circ$ ), 413 ( $r = 70 \text{ km}$ ,  $\theta = 45^\circ$ ) and S ( $r = 45 \text{ km}$ ). See Fig. 1 for node locations.

The normal component of horizontal velocity solution  $u$  and  $v$  obtained from

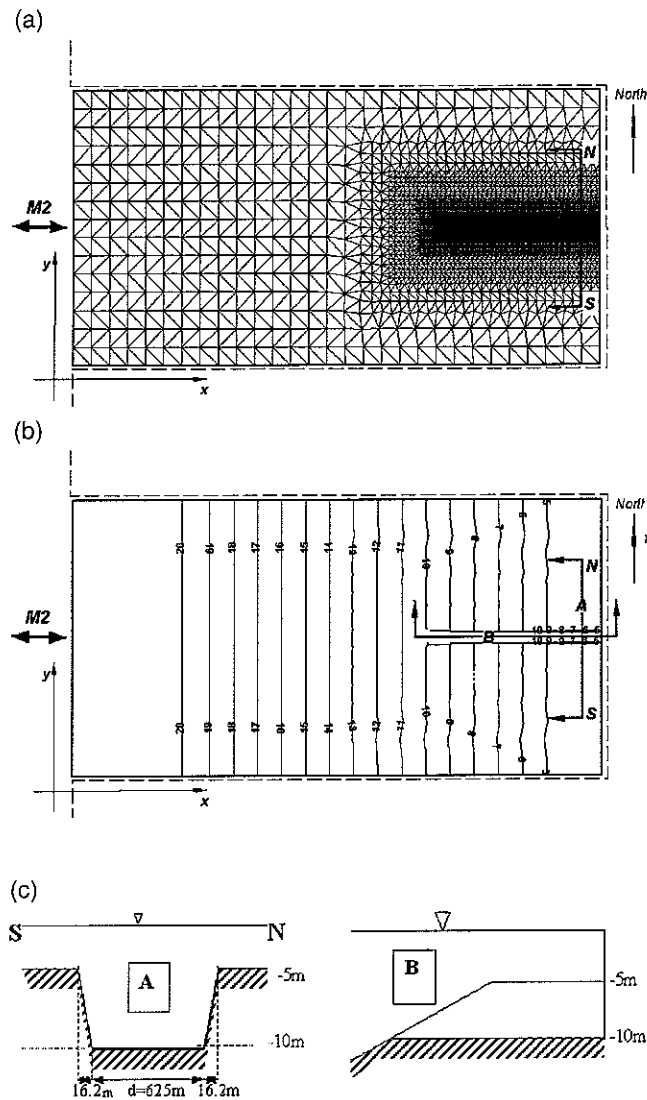


Fig 3 (a) Finite element grid of Rectangular Basin with Idealized Ship Channel (RBSC) The N and S indicate Northern and Southern part of the channel (b) The channel is located in the east-end side of the basin with a uniform 10m contour depth and 625 m wide A dashed-polygon represents mainland lateral boundary (c) The cross section of the RBSC with one-third-slope gradient at both sloping banks (section A) and a view of along channel section B Location of sections A and B are indicated in the figure part (b)

ADCIRC 3D-DSS model, as shown in Fig. 4a, is in fair agreement with the analytical solution except the near bottom, where the numerical solution gives smaller horizontal velocities than the analytical. This is probably because of the different approach applied in the solution. The numerical solution computes horizontal velocity solution directly from shear stress by integrating from bottom up, while the analytical solution applies linearized horizontal momentum equation in periodic form, in which a stress boundary condition is enforced at the surface. However, the solution between the node at  $\theta = 8.4^\circ$  and  $45^\circ$  give nearly similar solution indicating that the solution is independent on  $\theta$ . They differ in order of  $10^{-6}$ , indicating that consistent solutions have been performed.

Fig. 4b depicts the normal components of horizontal velocity from the deeper node (D) through the shallower node (S) at around maximum current period (i.e.  $\eta \approx 0$ ). Maximum current occurs in the middle of the domain, in this case at  $r = 70$  km, which is consistent with the conservation of mass for the flow propagating into the shallower water. However, the minimum current occurred at node S caused by the effect of the no-flow lateral boundary.

The solutions of vertical velocity for QATP are represented at the four nodes: node D, nodes 400 and 413 (both at  $r = 70$  km) and node S as shown in Fig. 1. The corresponding analytical solutions for those three profiles are also computed and compared in Fig. 5. Fig. 5a is taken at the beginning of one tidal cycle (i.e. tidal current  $\approx 0$ ) with  $r = 70$  km, while Fig. 5b and c are taken at maximum tidal current (i.e.  $\eta \approx 0$ ). Although the numerical solution indicates a slightly higher value than the analytical, in general the solution is in good agreement with the analytical solution. At the beginning of the tidal cycle, near the bottom, the numerical solution provides a lower velocity, which might be caused from the misfit of horizontal velocity solutions.

Points referenced here are similar to the points used by Muccino et al. (1997) and Luettich et al. (2002) for comparison of the three-dimensional models to the analyti-

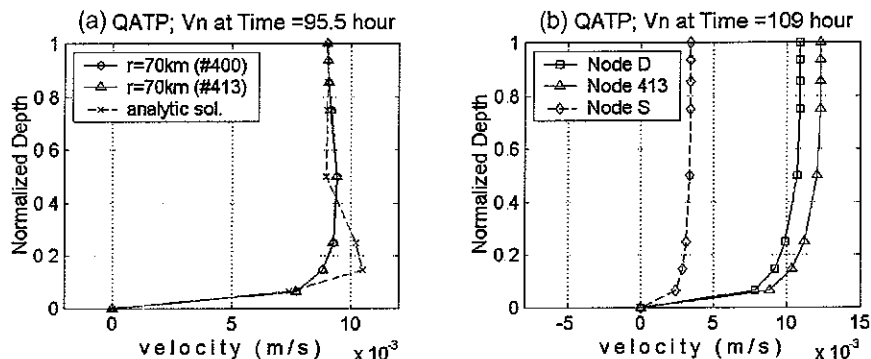


Fig. 4 (a) Amplitude of normal (horizontal) velocity at  $r = 70$  km around one-eighth of a tidal cycle obtained from numerical solutions, and compared to the analytical solution (b) Amplitude of normal (horizontal) velocity during maximum downstream current at  $t = 109$  h along radial section for  $\theta = 45^\circ$  at point D, 413 and S indicated in Fig. 1a. No analytic solution is available for this case.

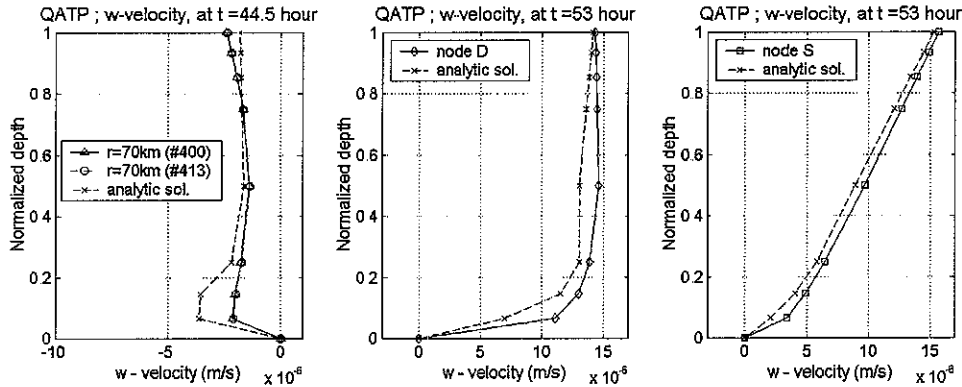


Fig. 5 Amplitude of vertical velocity solutions at various points and time stamps compared with the analytical solution: (a) at  $r = 70$  km near beginning of tidal cycle  $t = 44.5$  h, (b) at node D, and (c) at node S, both at maximum upstream current  $t = 53$  h

cal solutions, but their horizontal velocity solutions are obtained from FUNDY5 model. The results in this study are in good agreement with their results

An interesting result is the three-dimensional profile of the flow along the radial distance Fig 6 shows two 3D profiles at  $\theta = 8.4^\circ$  and  $\theta = 45^\circ$ , with the arrows indicating the direction of flow and the contour lines indicating the magnitude of vertical velocity. Both profiles are quite similar and consistent providing independent

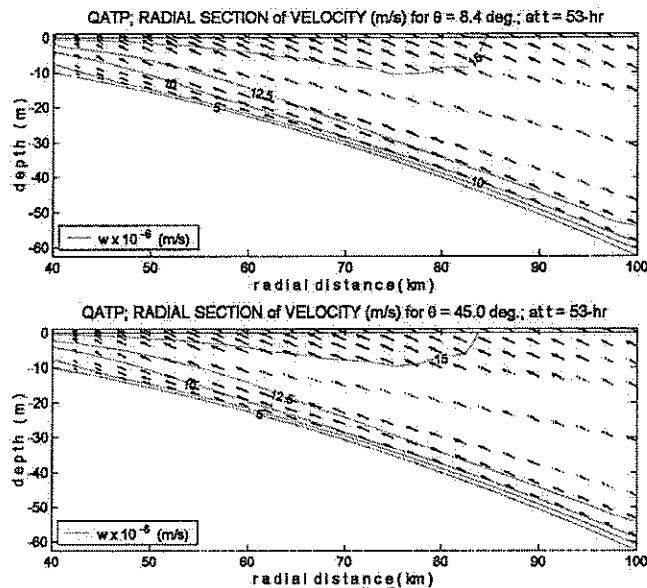


Fig 6 Radial section of velocity vector (arrows) at maximum upstream current  $t = 53$  h at (a) node 400 or  $\theta = 8.4^\circ$ , and (b) node 413 or  $\theta = 45^\circ$  Contour lines indicate the magnitude of vertical velocity

solutions on  $\theta$ . Consistent profiles (not shown) were also obtained for other  $\theta$  values, with a slight difference in vertical velocity values that is likely due to numerical round off error.

The near bottom profile follows the bathymetric profile, while the near surface flow tracks the free surface boundary conditions associated with the sea surface tidal cycle. Near the left end of the closed boundary the vertical velocity becomes significant in the flow field. Due to the presence of the wall, the horizontal current is quite small in the order of magnitude of the vertical velocity. Therefore, solving the vertical velocity in this region provides important information for better understanding of the flow as in near coastal, waterway or estuary zones.

The results of QATP have shown that the numerical model provides a reasonable three-dimensional velocity, and it is in accordance with the provided analytical solution. However, the horizontal velocity solution of ADCIRC 3D-DSS model exhibits doubtful results in the nodes near the lateral closed-boundary at both  $\theta = 0^\circ$  and  $\theta = 90^\circ$ . It is likely that the model will give zero tangential velocity along circular sections; but as shown in Fig. 7a, the numerical results experience a significant tangential velocity mainly around the nodes near the lateral boundary. The plot is taken at maximum tidal current, at time 53 h, and along radius  $r = 70$  km. The arrows in Fig. 7a indicate the direction of the flow in tangential-direction, while the contour lines in the left figure represent vertical velocity and in the right figure represent tangential velocity.

The maximum tangential velocity occurred at perimeter distance less than 10 km (i.e.  $\theta > 81^\circ$ ) and beyond 100 km (i.e.  $\theta < 9^\circ$ ), whereas the near zero tangential velocity is mostly found in the center of grid domain. The maximum tangential velocity is of order of  $2 \times 10^{-5}$  m/s, which is comparable to the magnitude of vertical velocity,  $w$ , with its maximum value around  $1.5 \times 10^{-5}$  m/s. The cause of the tangential flow is hypothetically due to the presence of the lateral boundary, but how they are generated in the model is not known yet, but it becomes an interesting problem to be further investigated. The effect of the tangential velocity in terms of the model stability for longer period of time and how those flows may affect the 3D velocity solution is under investigation.

For further investigation, the Annular test problem (ATP) is introduced with the grid geometry shown in Fig. 2, and similar numerical configuration to the QATP case, but the lateral land boundaries at  $\theta = 0$  and  $\theta = \pi/2$  are removed. In the normal (radial) direction, the results are almost similar to the profiles obtained in the QATP. There is a significant difference in tangential direction, however. In Fig. 7b, for  $r = 70$  km indicated by dashed-bold circle in Fig. 2, the tangential and vertical velocity profiles of ATP are provided for comparison to those of QATP in Fig. 7a.

The profiles of vertical velocities,  $w$ , are almost the same as their maximum around  $1.5 \times 10^{-5}$  m/s. However, the tangential velocity,  $v_\theta$ , has been reduced significantly from the order of  $2 \times 10^{-5}$  m/s in the QATP case (Fig. 7a) to the order of  $1.5 \times 10^{-7}$  m/s in the ATP case (Fig. 7b), which becomes insignificant to the vertical velocity magnitude. The tangential velocity is perhaps caused by round off error during numerical computation. The error carried by horizontal velocity solutions, though not significant in terms of horizontal velocity, may lead to critical

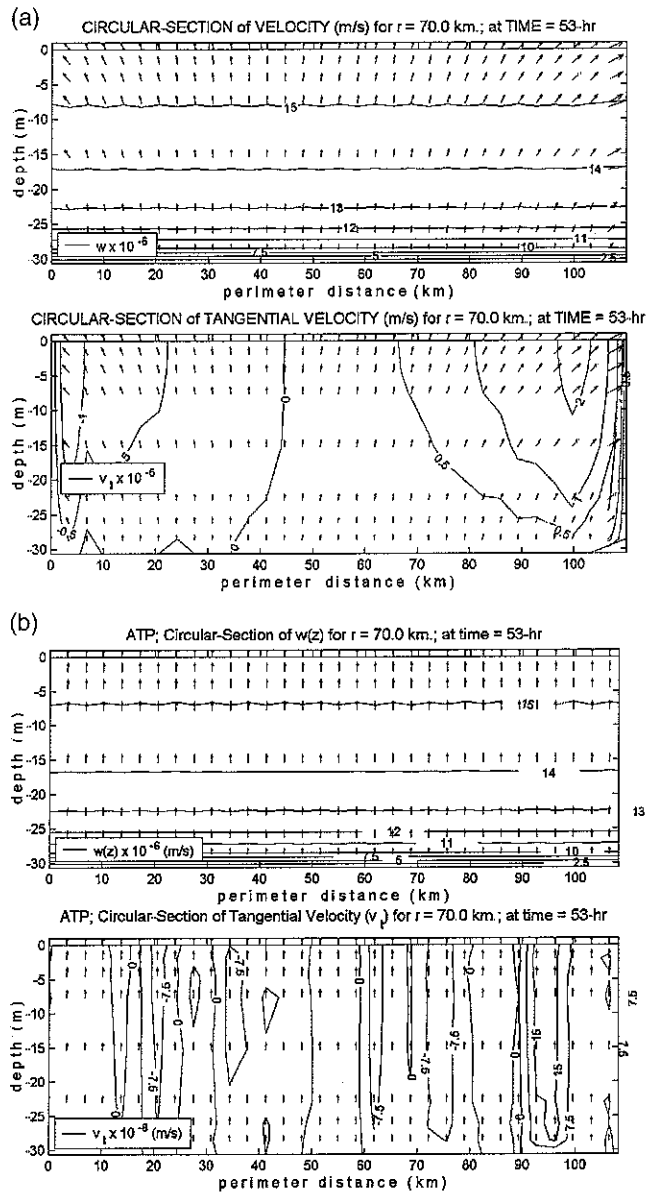


Fig 7. (a) Circular-section of tangential velocity vector (arrows) at maximum upstream current  $t = 53$  h at radius  $r = 70$  km for QATP Contour lines represent vertical velocity (upper) and tangential velocity (lower) (b) A quarter of circular-section of tangential velocity vector (arrows) at maximum upstream current  $t = 53$  h at radius  $r = 70$  km for ATP Contour lines represent vertical velocity (upper) and tangential velocity (lower)

value in term of vertical velocity computation since the vertical solution deals with a very small number in order of 1/1000 of the horizontal solution. Thus, accurate horizontal velocity solutions are extremely important in order to obtain a reasonable vertical velocity solution

The very mild slopes in the QATP and ATP examples do not produce large vertical velocities. Thus very accurate horizontal solutions are necessary.

4.2 Rectangular basin with ship channel (RBSC)

A step toward a realistic coastal problem is to investigate the ability of the model to solve a “steep” channel problem. The finite element grid and bathymetric contour of the channel are shown in Fig. 3. Five nodes are selected to represent the channel as: south-top, south bottom, north-top, north-bottom and center. The top and bottom nodes are located in the top and bottom of the channel slope respectively. The center node is located exactly in the center of the channel. The slope gradient is 1:3, which is comparable to the typical dredged ship channel.

Fig. 8 represents the water level  $\eta$  and depth averaged velocity  $U$  and  $V$  for 60

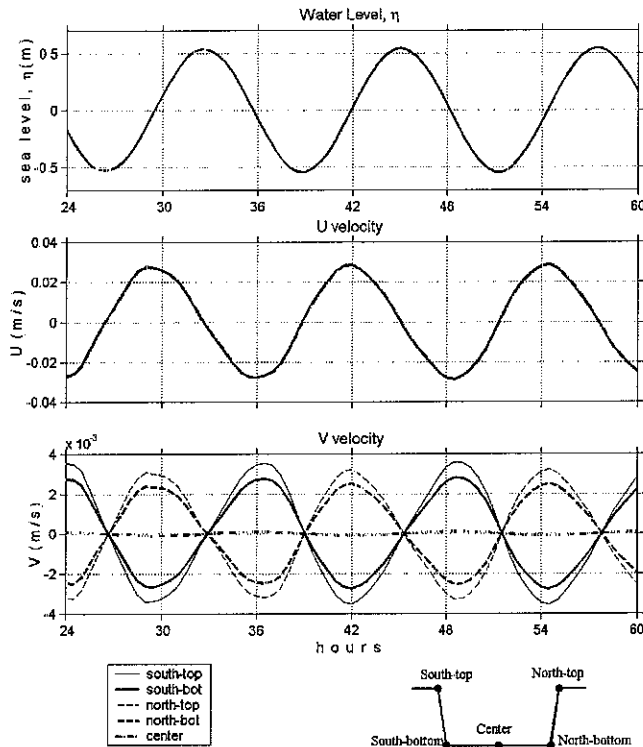


Fig. 8 Plot of (a) sea level height,  $\eta$ , (b) depth-averaged velocity  $U$ , and (c) depth averaged velocity  $V$ , for five selected points across the channel in RBSC case: (1) south-top, (2) south-bottom, (3) center (4) north-bottom and (5) north-top (see figure index for locations). The profiles for these five points are coincident for  $\eta$  and  $U$  solutions, but nearly symmetrical for  $V$ .

h model runs Positive values in the figure indicate sea level rise for  $\eta$ , up stream current for  $U$  and northward flow for  $V$

The water level in the five selected nodes are almost coincident They differ up to  $1.5 \times 10^{-5}$  m Two selected times for presentation at  $t = 45$  and  $t = 54.5$  h represent maximum tidal level (i.e. near zero current velocity) and nearly zero tidal (i.e. near maximum upstream current) respectively. The model also produces a nearly uniform  $U$  velocity, with their maximum difference at about  $0.4 \times 10^{-3}$  m/s between the top-slope and center-nodes

The tangential velocity (i.e.  $V$  component) occurs nearly symmetric to the center. The top-slope and bottom-slope pair nodes are in opposite signs with nearly the same magnitude The center node varies alternately to the north and south direction in the order of  $1 \times 10^{-5}$  m/s with a nearly zero time average tangential velocity. An inward tangential flow (to the center) occurs during downstream current and inversely an outward tangential flow occurs during upstream flow. A more clear view of the flow direction vertically around the channel is given in Fig. 9a and b. The no-slip condition at the bottom forces zero velocity at the bottom in both directions. The conditions in the figure are for maximum upstream tidal current at  $t = 54.5$  h. Again, in Fig. 9a it is shown that the  $u$ -velocity is almost uniform across the channel consistent with the  $U$  component where all five selected points are nearly coincident.

Meanwhile, the  $v$ -velocity depicts similar pattern to the  $V$  component (Fig. 9b) with an outward tangential flow during upstream current. However, it is clearly seen in this vertical profile of the horizontal velocity that the unsymmetrical tangential flows exist although the Coriolis force has been turned off in the numerical model. The maximum difference of this flow between north and south is about  $5 \times 10^{-4}$  m/s. Those discrepancies may lead to a significant difference in the vertical velocity solutions. The shape and orientation of the finite element may contribute to this problem, but it needs to be investigated further.

The time series of vertical velocity at the selected five nodes across the channel slope and channel is shown in Fig. 10. The series are taken between  $t = 24$  h and  $t = 60$  h at three depths: surface, mid-layer and near bottom. The vertical velocities

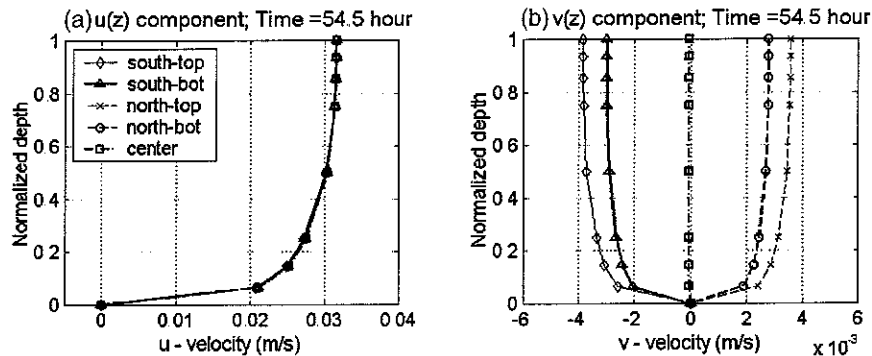


Fig. 9. Vertical profile of horizontal velocity solutions,  $u$  (left) and  $v$  (right), for the five selected points in the channel at around maximum upstream tidal current.

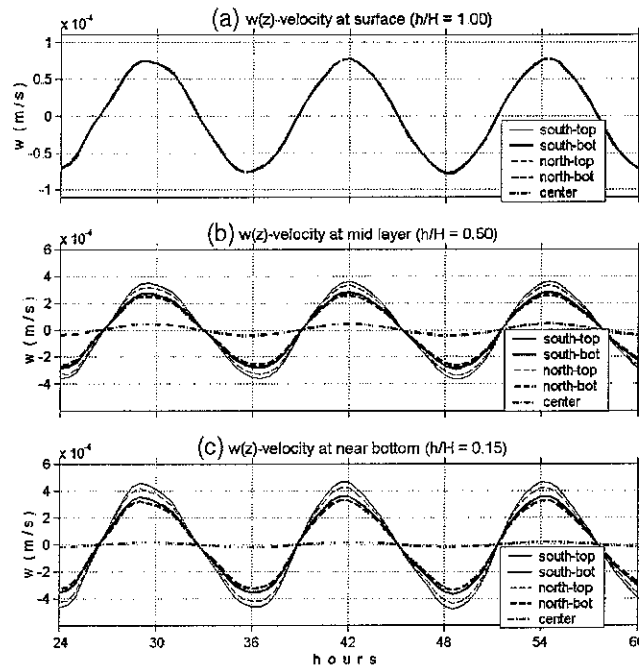


Fig. 10. Representations of time series of vertical velocity,  $w(z)$ , for the five selected points at three depths layers: (a) surface,  $h/H = 1.0$ , (b) mid-depth,  $h/H = 0.5$  and (c) near-bottom,  $h/H = 0.15$

at the surface for all nodes satisfy the free surface boundary condition. The series are nearly coincident for all nodes, since the sea surface variation across the channel is relatively small.

In the mid-layer, the figure shows a vertical velocity up to the order of  $4 \times 10^{-4}$  m/s even though the horizontal velocity is quite small or nearly zero at the center. The maximum vertical velocity occurs at near bottom layer. The presence of channel slope mainly contributes to the magnitude of vertical velocity at this layer. Around the maximum upstream current, say at  $t = 54.5$ , the vertical velocity values at near bottom increase significantly up to  $4.8 \times 10^{-4}$  m/s, or  $\sim 35$  m/day. In terms of sediment fall velocity, this value will be important. For example, the typical sediment fall velocity for fine sand, 0.1 mm, is 0.001 m/s (Kamphuis, 2000). The vertical velocity value thus contributes up to 48% of the typical fall velocity.

The vertical profiles of vertical velocity are unsymmetrical between north and south pair nodes. The south nodes tend to produce slightly larger values than that of the north nodes up to  $10^{-5}$  m/s even though the model does not include the Coriolis force. As it was discussed before, these discrepancies are probably contributed from the unsymmetrical tangential velocity solution.

A cross section given in Fig. 11a shows the distribution of tangential velocity across the channel at time  $t = 54.5$  h. It is shown that the maximum outward flow takes place around the slope, and is nearly zero near the center. From the slope, the velocities gradually decrease outward from the channel. Correspondingly, the

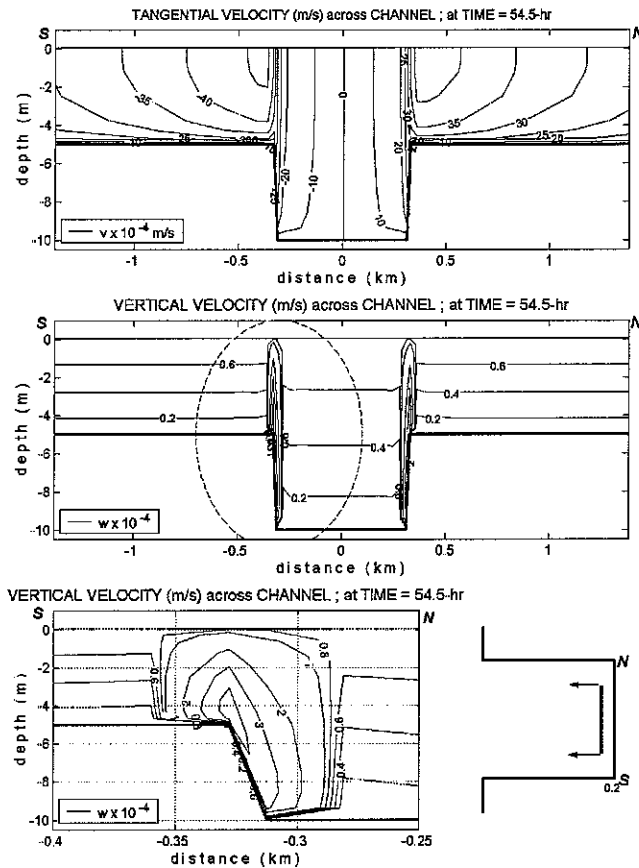


Fig 11. (a) Contour plot of tangential ( $v$ ) velocity across the channel Location of cross section of channel is specified in Fig 3 (b) Contour plot of vertical velocity ( $w$ ) across the channel (c) Exaggerated contour plot of the vertical velocity around the southern channel slope as indicated by a dashed circle in the figure of part (b) The x-axis indicates a distance from the center of the channel, and y-axis is for depth

maximum vertical velocity also occurs around the slope (Fig 9b). Exaggeration of the figure at the southern slope (marked by a dashed circle) is also displayed in Fig. 9c The vertical velocities beyond the slope area are relatively small, in the order of  $10^{-6}$  m/s. However, at the slope, the vertical velocity increases significantly up to 0.48 mm/s

**5. Concluding remarks**

An improvement in three-dimensional ADCIRC 3D-DSS model has been made to include the vertical velocity solution. Comparison to the analytical solutions and numerical results of other researchers in most cases are in good agreement The accuracy of vertical velocity solution is critically dependent on the accuracy of the

horizontal velocity solution. At some points from the QATP case, mainly in the region near the lateral boundary at  $\theta = 0$  and  $\theta = \pi/2$ , the presence of tangential velocity may lead to over-determined vertical velocity solution. The order of the tangential velocity in this region is nearly in the same order as the vertical velocity.

In another experiment, the ATP case removes the presence of those lateral boundaries. For this case at  $r = 70$  km, the model demonstrates a significantly reduced tangential velocity near the “boundary” down to the order of  $10^{-7}$  m/s. More uniform vertical flows along the circular section has been achieved in Fig. 7b (ATP) rather than the profiles in Fig. 7a (QATP). However, the cause of that tangential flow near the boundary has not been well studied yet. Practically it is recommended to define a boundary region many kilometers away from the specific area of study.

The experiment on the RBSC grid produces significant vertical velocity in the region around the slope of an idealized ship channel. The model is driven by an  $M_2$  tidal component with amplitude of 0.5 m in the open boundary. The maximum vertical velocity may reach approximately 0.5 mm/s along the slope of the channel that is comparable up to 50% of the settling velocity of fine sand. This model promises to provide a working tool for studies of sediment movement when combined with deposition and suspension processes.

### Acknowledgements

This study has been supported in part by the US Environmental Protection Agency through the South and Southwest Hazardous Substance Research Center and the National Science Foundation.

### References

- Grenier, R.R. Jr., Luettich, R.A. Jr., Westerink, J.J., 1995. A comparison of the nonlinear frictional characteristics of two-dimensional and three-dimensional models of a shallow tidal embayment. *J. Geophys. Res.* (C7) 100 (C6), 13719–13735.
- Kamphuis, J.W., 2000. *Introduction to Coastal Engineering and Management*, Advanced Series on Ocean Engineering, vol. 16. World Scientific, Singapore.
- Luettich, R.A. Jr., Muccino, J., 2001. Summary of Vertical Velocity Calculation Methods as Considered for 3D ADCIRC Hydrodynamic Model, Paper presented on ADCIRC Meeting 20-21 Feb 2001, NRL, Stennis, Mississippi.
- Luettich, R.A. Jr., Muccino, J.C., Foreman, M.G.G., 2002. Considerations in the Calculation of Vertical Velocity in Three-Dimensional Circulation Models. *Journal of Atmospheric and Oceanic Technology*; submitted.
- Luettich, R.A. Jr., Hu, S., Westerink, J.J., 1994. Development of the direct stress solution technique for three-dimensional hydrodynamic models using finite element. *Int. J. Num. Meth. Fluids* 19, 295–319.
- Luettich, R.A. Jr., Westerink, J.J., 2001. Formulation and Numerical Implementation of the 3D ADCIRC Finite Element Model Version 36.01.
- Luettich, R.A. Jr., Westerink, J.J., Scheffner, N.W., 1992. ADCIRC: An advanced Three-Dimensional Circulation Model for Shelves, Coasts, and Estuaries. Report 1, Technical Report DRP-92-6, Dredging Res. Prog., USACE, Washington DC.
- Luettich, R.A. Jr., Westerink, J.J., Scheffner, N.W., 1992. ADCIRC: An advanced Three-Dimensional

- Circulation Model for Shelves, Coasts, and Estuaries Report 2, Technical Report DRP-92-6, Dredging Res. Prog, USACE, Washington DC
- Lynch, D.R., Officer, C.B., 1985. Analytic test case for three-dimensional hydrodynamic models. *Int J Num. Meth. Fluids* 5, 529–543.
- Martin, J.L., McCutcheon, S.C., 1998. In: Schottmann, R.W. (Ed.), *Hydrodynamics and Transport for Water Quality Modeling*. Lewis Publisher, Washington, DC.
- Mellor, G.I., 1998. User Guide for a Three-Dimensional, Primitive Equation, Numerical Ocean Model, Prog. In Atmospheric and Ocean Sciences, Princeton Univ., Princeton, NJ.
- Muccino, J.C., Gray, W.G., Foreman, G.G., 1997. Calculation of vertical velocity in three dimensional, shallow water equation, finite elements model. *Int J Num Meth Fluids* 25, 779–802.